Ultrasonics 94 (2019) 65–73

Contents lists available at ScienceDirect

Ultrasonics

journal homepage: www.elsevier.com/locate/ultras

Doppler shift equation and measurement errors affected by spatial variation of the speed of sound in sea water

Shokichi Tanaka[a,*], Hideyuki Nomura[a], Tomoo Kamakura[b]

[a] Graduate School of Informatics and Engineering, The University of Electro-Communications, 1-5-1 Chofugaoka, Chofu-shi, Tokyo 182-8585, Japan
[b] Center for Industrial and Governmental Relations, The University of Electro-Communications, 1-5-1 Chofugaoka, Chofu-shi, Tokyo 182-8585, Japan

ARTICLE INFO

Keywords:
Ultrasonic Doppler device
Doppler effect
Speed of sound
Improved Doppler shift equation
Measurement error

ABSTRACT

Underwater ultrasonic devices using the Doppler effect generally presuppose that the speed of sound is uniform in a propagation medium. Actually, however, the speed of sound in the sea varies with water depth, so that the assumption of such uniform speed has the potential to cause measurement errors. The present study is then involved in theoretically improving the conventional Doppler shift equation by taking into account the fact that the speed of sound is dependent on the propagation path. The study also evaluates measurement errors caused by spatial variation in the speed of sound. Interestingly, the theory predicts that only the speeds of sound at a sound source position and the target position affect the Doppler shift, and the error of the target speed, which is the value that is ultimately measured in ultrasonic Doppler devices, is inversely proportional to the ratio of the speed of sound near the target to that near the source. In order to validate the improved Doppler equation, experiments are conducted using a water tank. The measured Doppler shift data are in agreement with the theoretical predictions within the order of a few tens of hertz.

1. Introduction

The purpose of the present study is to investigate Doppler shift equation for expanding the scope of applicability according to actual sea environments. As is well known, the Doppler effect is a phenomenon that usually occurs with waves of all types, such as sound, radio, and light waves. Its application field is then wide, and the devices to which it is applied are diverse. In underwater acoustics, devices using the Doppler effect include Doppler navigation sonars, which measure the speed of a ship relative to the sea bottom; Doppler current profilers [1]; and Doppler velocity logs [2], which measure the ship speed relative to the water.

Incidentally, the equation of the Doppler shift used in these underwater ultrasonic devices conventionally assumes that the speed of sound in water is uniform in a propagation medium, although the speed is usually corrected according to the measured temperature of the water around the ultrasonic transducers [3]. In actual sea environments, however, the speed of sound varies spatially, mainly because of the spatial non-uniformity of temperature, pressure, and salinity in sea water, which are functions of water depth [4]. For example, depending on the ocean area and the season, the speed of sound at a depth of several hundred meters is typically reduced by a few percent relative to the speed near the sea surface. Hence, assuming a uniform speed of sound may cause measurement errors when predicting the speed of a ship or the current velocity using the conventional Doppler shift equation. Moreover, Doppler shift is one of the main factors that degrade communication quality in underwater acoustics [5], so that a deeper understanding of Doppler shift and research on communication methods to suppress the degradation will be closely related.

The main interests of the present study are twofold. One is to derive the equation of the Doppler shift by taking into account the fact that the speed of sound is actually dependent on the propagation path. In order to derive the equation, the theory starts the expansion and contraction of the time width of a sound pulse that occur during its propagation. In addition, measurement errors arising in the conventional Doppler equation is derived quantitatively by comparison with the improved equation. The measurement errors of the target speed, which is the value ultimately being measured, are also evaluated using the ratio of the speed of sound near the source to the speed of sound near the target.

The other interest is to validate the improved Doppler shift by experiment. A water tank is separated into two sub-tanks by a partition board. A 2-MHz piezoelectric transducer that transmits tone-burst ultrasound pulses is located in one sub-tank. The transducer can also receive echoes from a target in another sub-tank. Motion toward the transducer is given to the target. The speed of sound around the transducer and the speed of sound around the target are controlled by

* Corresponding author.
E-mail addresses: shokichi.tanaka@uec.ac.jp (S. Tanaka), h.nomura@uec.ac.jp (H. Nomura), tomoo.kamakura@smart-ae.jp (T. Kamakura).

https://doi.org/10.1016/j.ultras.2018.12.002
Received 8 June 2018; Received in revised form 13 November 2018; Accepted 2 December 2018
Available online 11 December 2018
0041-624X/

independently changing the water temperatures of the two separated tanks. The Doppler shifts in the received pulses are measured while changing the speeds of sound and are carefully compared with the theoretical predictions using the improved Doppler shift equation.

2. Improved Doppler shift equation

The new derivation of the Doppler shift equation is based on the situation that occurs when a tone burst pulse with time width T is transmitted from a sound source (transducer) toward a target that is moving relative to the source, reflected by the target, and finally received at the same source. In this process, the pulse travels through a propagation medium in which the speed of sound varies spatially.

When the transmitting burst pulse is a sinusoidal signal of frequency f with N cycles, N is given by Tf. Since N is unchanged during propagation, the frequency of the pulse is inversely proportional to T. Thus, the Doppler shift (i.e., the difference between the transmitting and receiving frequencies) can be derived from the reciprocal of the expansion and contraction of the pulse time width, T, generated along the propagation path.

In order to obtain T, we examine in detail the time difference between the propagation paths of the leading and trailing edges of the pulse. As discussed later, two propagation paths that are related to the wave going from the source to the target and the wave returning from the target can each be divided into a common propagation path and an edge-dependent propagation path. Here, the expansion and contraction of the pulse does not occur along the common propagation path because the total propagation times along the path are the same for the leading and trailing edges.

In addition to the non-uniform propagation medium, the speed of sound changes substantially even for a medium with nonzero velocity, so that the ocean current may affect the measurement accuracy of the Doppler shift. As such, in the present study, we assumed that an ocean current exists.

2.1. Expansion and contraction of the pulse time width

For simplicity, let us consider a 1D propagation model such that sound source (transducer) S is located at P and target T_g is located at Q with distance d_0 between them at time $t = 0$ and that S and P move in the z-direction, as shown in Fig. 1. The origin of the z-axis is at the sound source, and the positive z-direction is toward target T_g. The sound source and target move at different speeds, v_s and v_t, respectively, such that $v_s < v_t$. Hereinafter, suffixes s and t indicate the source and the target, respectively. The speed of sound, c, as well as the z-component of the ocean current speed, u, are generally dependent on the depth, i.e., the distance z from the sound source. Components v_s, c_s, u_s, v_t, c_t, and u_t are assumed to be independent of time.

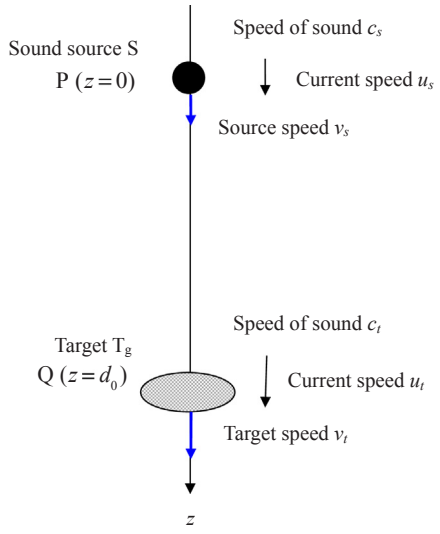

Fig. 1. 1D model of sound source S and target T_g.

The conventional Doppler shift, Δf_{con}, with a spatially constant speed of sound, c_s, in a propagation medium is given as

$$\Delta f_{con} = 2\frac{v_s - v_t}{c_s}\cdot f, \tag{1}$$

where f is the transmission frequency. When the 1D model is not satisfied (i.e., when the moving direction of the sound source and the target is not coincident with that of the wave propagation), the direction cosine, $\cos\theta$, must be multiplied by the right-hand side of Eq. (1), where θ is the angle between the direction of the moving sound source or the target and that of the wave propagation [6].

Suppose that a tone burst pulse with time width T is radiated toward target T_g from sound source S at time $t = 0$. After time $t\ (> 0)$, position z_P of the sound source moves at v_s and is given by

$$z_P = v_s\cdot t. \tag{2}$$

The position of the target, z_Q, also moves at v_t to

$$z_Q = d_0 + v_t\cdot t. \tag{3}$$

The position of the leading edge of the pulse, z_l, is expressed as

$$z_l = \{c(z) + u(z)\}\cdot t. \tag{4}$$

Under the assumption that z_l is equal to z_Q, it is possible to calculate time T_A at which z_l reaches target T_g.

The position of the trailing edge of the pulse, z_t, is expressed as

$$z_t = v_s\cdot T + \{c(z) + u(z)\}\cdot(t - T), \quad (t \geqslant T). \tag{5}$$

Likewise, setting $z_t = z_Q$ yields time T_B, at which z_t reaches target T_g.

Fig. 2 shows the situation for generating T_A and T_B and the corresponding propagation paths z_l and z_t in the t–z coordinate system. The propagation paths (i.e., the propagation trajectory) of z_l and z_t are denoted as P_1 and P_2, respectively. Since the speed of sound, $c(z)$, and the current speed, $u(z)$, are functions of z, the propagation paths, P_1 and P_2, are generally tilted lines, the inclinations of which vary spatially, i.e., wiggling lines. In reality, $u(z)$ in actual sea environments is at most a few m/s, whose magnitude is much smaller that of the sound speed $c(z)$, approximately 1500 m/s. The wiggling curves in Fig. 2 are then exaggerated for clarity.

Likewise, the speeds v_s and v_t of the source and target are both a few m/s. Accordingly, the inclinations of the propagation paths P_1 and P_2 in the t–z coordinate system are approximately three orders of magnitude larger than those of the trajectories of the sound source and target positions, z_P and z_Q. It should be noted that the inclinations of P_1 and P_2 are quite larger than those of z_P and z_Q in actual situation.

A comparison of lines P_1 and P_2 demonstrates that the curved lines have edge-dependent propagation paths. The lines in the vicinity of the sound source and the target are highlighted in bold red. As explained previously, the change in the propagation times of z_l and z_t generated along these different edge-dependent propagation paths causes the expansion and contraction of time width T, producing the Doppler effect [7]. The expansion and contraction generated by these two edge-dependent propagation paths are derived below.

The pulse time width when the pulse reaches the target is denoted as T', as shown in Fig. 2, and becomes

$$T' = T_B - T_A. \tag{6}$$

Moreover, when the pulse passes through position z on the common propagation path (i.e., P_1 and P_2 are excluded in the edge-dependent propagation paths), the pulse width is denoted as T_f, which is constant regardless of z and takes the form

$$T_f = T - \Delta T_1, \tag{7}$$

where ΔT_1 is the propagation time generated along the edge-dependent

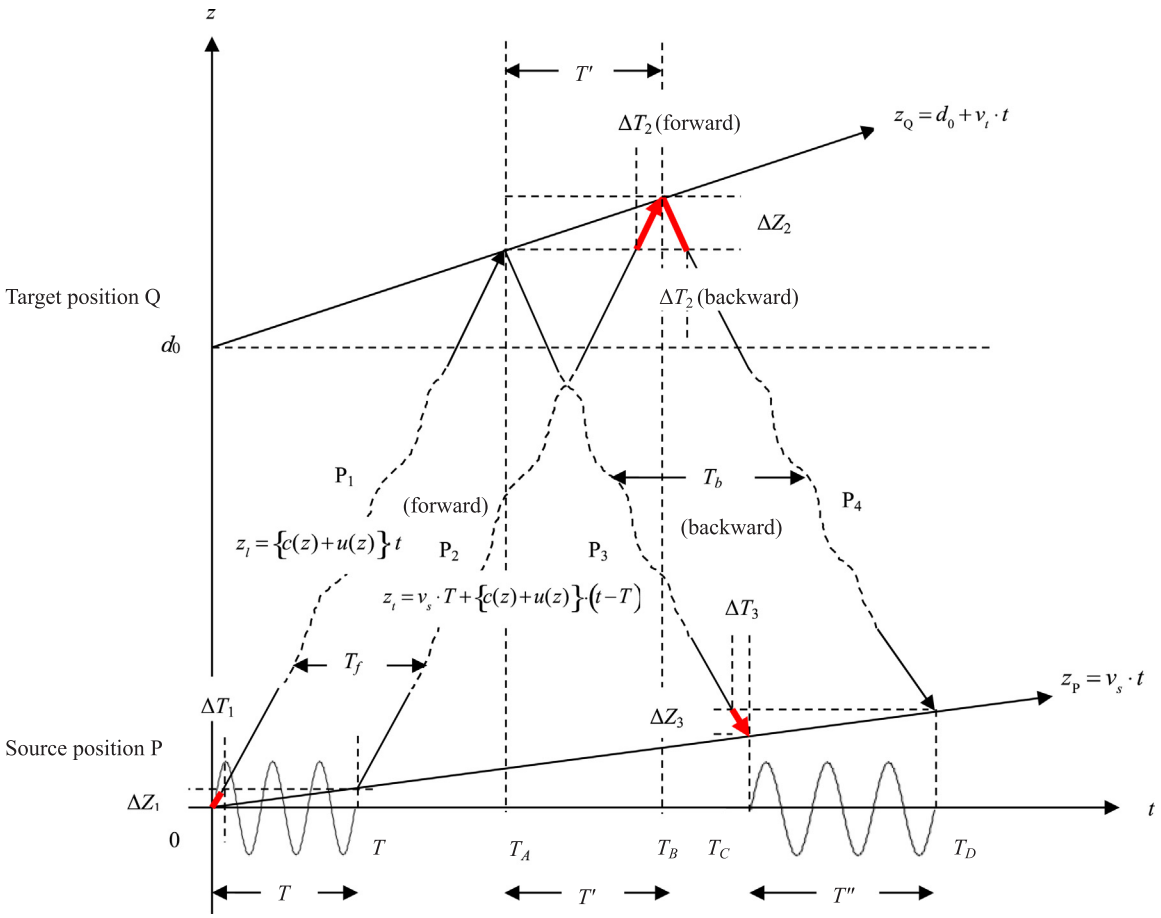

Fig. 2. Propagation paths of z_l and z_t in the t–z coordinate system ($N = 3$, $v_s < v_t$). In reality, the inclinations of P_1, P_2, P_3, and P_4 are much larger than those of z_P and z_Q. Since $c(z)$ and $u(z)$ are functions of z, P_1, P_2, P_3, and P_4 become curved lines, i.e., wiggling lines.

propagation portion of P_1 in the vicinity of the sound source and is given by

$$\Delta T_1 = \frac{\Delta Z_1}{c_s + u_s} = \frac{v_s \cdot T}{c_s + u_s}. \tag{8}$$

In Eq. (8), ΔZ_1 is the propagation distance corresponding to ΔT_1.

Substituting Eq. (8) into Eq. (7) yields

$$T_f = \frac{c_s + u_s - v_s}{c_s + u_s} \cdot T. \tag{9}$$

Likewise, ΔT_2 (forward) and ΔZ_2 are the increments in the propagation time and the corresponding propagation distance, respectively, generated along the edge-dependent propagation path P_2 in the vicinity of the target. The forward propagation speed of the wave is $c_t + u_t$, whereas the backward propagation speed is $c_t - u_t$. Hence, ΔT_2 (forward) must be distinguished from ΔT_2 (backward). For simplicity, a local coordinate system is introduced based on a triangle configuration in the vicinity of the target along P_2, as shown in Fig. 3, to obtain the intersection $(T', \Delta Z_2)$ of z_Q and z_t. The position of the trailing edge, z_t, in Fig. 3 is given by

$$z_t = (c_t + u_t) \cdot (t - T_f). \tag{10}$$

From Eqs. (2) and (10), the intersection coordinates $(T', \Delta Z_2)$ of z_Q and z_t can be obtained

$$T' = \frac{c_t + u_t}{c_t + u_t - v_t} \cdot T_f, \tag{11}$$

$$\Delta Z_2 = v_t \cdot T' = v_t \cdot \frac{c_t + u_t}{c_t + u_t - v_t} \cdot T_f. \tag{12}$$

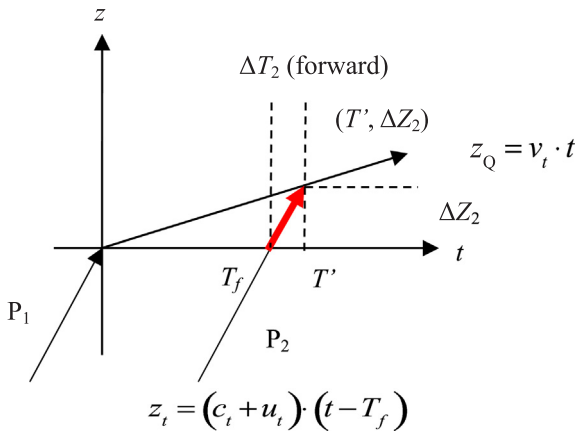

Fig. 3. Local coordinate system in the vicinity of the target (forward).

Substituting Eq. (9) into Eq. (11) yields the pulse width at the target T' as

$$T' = \frac{c_t + u_t}{c_t + u_t - v_t} \cdot \frac{c_s + u_s - v_s}{c_s + u_s} \cdot T. \tag{13}$$

Eq. (13) describes the expansion and contraction of the pulse generated along P_1 and P_2. From Eqs. (9) and (13), ΔT_2 (forward) is obtained as

$$\Delta T_2(\text{forward}) = T' - T_f = \frac{v_t}{c_t + u_t - v_t} \cdot \frac{c_s + u_s - v_s}{c_s + u_s} \cdot T. \tag{14}$$

Next, we consider the expansion and contraction of the pulse generated on the returning propagation path. Here, P_3 and P_4 are the return paths

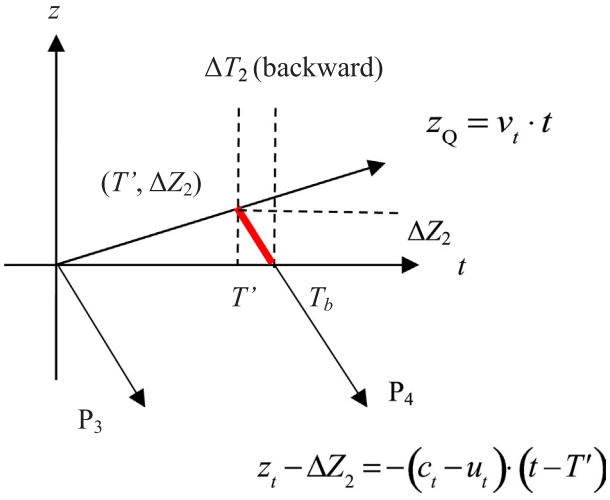

Fig. 4. Local coordinate system in the vicinity of the target (backward).

of z_l and z_t, respectively, and T_C and T_D are the times at which z_l and z_t, respectively, return to the sound source S. Finally, T'' is the pulse width when the pulse returns to the sound source:

$$T'' = T_D - T_C. \tag{15}$$

As before, the two edge-dependent propagation paths P_3 and P_4 in the vicinity of the target and sound source are highlighted. The derivation of the expansion and contraction generated by these edge-dependent propagation paths is as follows.

Both ΔT_2 (backward) and ΔZ_2 are the increases in the propagation time and the corresponding propagation distance, respectively, generated along edge-dependent propagation path P_4 in the vicinity of the target. When the pulse passes through position z on the common propagation path, the pulse time width, T_b, is constant regardless of position z. Based on the triangle configuration in the vicinity of the target on P_4, a second local coordinate system is shown in Fig. 4.

Positions z_Q and z_t of the target and the trailing edge of the pulse, respectively, intersect at (T', ΔZ_2). Here, the intersection (T_b, 0) of z_t and the t-axis is obtained. In this case, z_t is expressed as

$$z_t - \Delta Z_2 = -(c_t - u_t)\cdot(t - T'). \tag{16}$$

Setting $z_t = 0$, and solving t in Eq. (16) yields

$$T_b = \frac{c_t - u_t + v_t}{c_t - u_t}\cdot T'. \tag{17}$$

From Eq. (17), ΔT_2 (backward) is given by

$$\Delta T_2(\text{backward}) = T_b - T' = \frac{v_t}{c_t - u_t}\cdot T'. \tag{18}$$

Finally, the expansion and contraction of the pulse time width generated along the returning propagation path in the vicinity of the sound source are obtained. As before, ΔT_3 and ΔZ_3 are the decreases in the propagation time and propagation distance, respectively, generated along edge-dependent propagation path P_3 in the vicinity of the sound source. Fig. 5 shows a third local coordinate system based on the triangle configuration in the vicinity of the sound source along P_3.

Here, T'' is expressed as

$$T'' = T_b - \Delta T_3. \tag{19}$$

Position z_P of the sound source and the t-axis intersect at (T_b, 0) and the intersection (ΔT_3, ΔZ_3) of z_P and the position of the leading edge of the pulse, z_l, is obtained. In this case, z_P and z_l are given as follows:

$$z_P = v_s\cdot(t - T_b), \tag{20}$$

$$z_l = -(c_s - u_s)\cdot t. \tag{21}$$

Equating z_P and z_l yields ΔT_3:

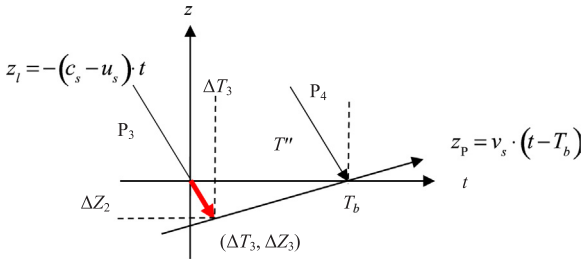

Fig. 5. Local coordinate system in the vicinity of the sound source.

$$\Delta T_3 = \frac{v_s}{c_s - u_s + v_s}\cdot T_b. \tag{22}$$

By substituting Eq. (17) into Eq. (22), ΔT_3 takes the form

$$\Delta T_3 = \frac{v_s}{c_s - u_s + v_s}\cdot\frac{c_t - u_t + v_t}{c_t - u_t}\cdot T'. \tag{23}$$

From Eqs. (13) and (19), T'' is given by

$$T'' = \frac{c_s - u_s}{c_s - u_s + v_s}\cdot\frac{c_t - u_t + v_t}{c_t - u_t}\cdot\frac{c_t + u_t}{c_t + u_t - v_t}\cdot\frac{c_s + u_s - v_s}{c_s + u_s}\cdot T. \tag{24}$$

Eq. (24) formulates the overall expansion and contraction of the pulse time width generated along P_1, P_2, P_3, and P_4. The form indicates the product of four fractions. From left to right, the fractions are the expansion or contraction of the pulse corresponding to ΔT_3, that corresponding to ΔT_2 (backward), that corresponding to ΔT_2 (forward), and that corresponding to ΔT_1.

Through the derivation process mentioned above, it is possible to obtain the same formula for the overall expansion and contraction of the pulse time width when the source and target are moving toward each other ($v_s > v_t$).

2.2. Derivation of the improved Doppler shift equation

Here, f'' is the frequency of the received pulse and is obtained as the reciprocal of T'', as given by Eq. (24):

$$f'' = \frac{c_s - u_s + v_s}{c_s - u_s}\cdot\frac{c_t - u_t}{c_t - u_t + v_t}\cdot\frac{c_t + u_t - v_t}{c_t + u_t}\cdot\frac{c_s + u_s}{c_s + u_s - v_s}\cdot f. \tag{25}$$

Based on the assumption that v_s, v_t, u_s, and u_t are generally much smaller than c_s and c_t, i.e., the first-order approximation of the Taylor series expansion, it follows that

$$\begin{aligned} f'' &= \left\{1 - \tfrac{(u_s - v_s)}{c_s}\right\}\left\{1 + \tfrac{u_s}{c_s} + \left(\tfrac{u_s}{c_s}\right)^2 + \cdots\right\}\left(1 - \tfrac{u_t}{c_t}\right)\left\{1 + \tfrac{(u_t - v_t)}{c_t} + \left(\tfrac{u_t - v_t}{c_t}\right)^2 + \cdots\right\} \\ &\times\left\{1 + \tfrac{(u_t - v_t)}{c_t}\right\}\left\{1 - \tfrac{u_t}{c_t} + \left(\tfrac{u_t}{c_t}\right)^2 - \cdots\right\}\left(1 + \tfrac{u_s}{c_s}\right)\left\{1 - \tfrac{(u_s - v_s)}{c_s} + \left(\tfrac{u_s - v_s}{c_s}\right)^2 - \cdots\right\}\cdot f \\ &= \left\{1 + \tfrac{2v_s}{c_s} - \tfrac{2v_t}{c_t} + (\text{more than second orders})\right\}\cdot f. \end{aligned} \tag{26}$$

Therefore, f'' is approximated as

$$f'' = \left\{1 + 2\left(\frac{v_s}{c_s} - \frac{v_t}{c_t}\right)\right\}\cdot f. \tag{27}$$

The improved equation for the Doppler shift, Δf_{imp}, is finally written as

$$\Delta f_{imp} = 2\left(\frac{v_s}{c_s} - \frac{v_t}{c_t}\right)\cdot f. \tag{28}$$

From Eq. (28), we have the following:

(i) Only the speeds of sound at the source and the target, c_s and c_t, affect the Doppler shift.
(ii) The speeds of ocean currents, u_s and u_t, do not generally affect the Doppler shift.
(iii) The speeds v_s and v_t of the source and target are coupled with the corresponding speeds of sound in the surrounding water, c_s and c_t. When v_s is zero, the Doppler shift is independent of c_s. Similarly, the Doppler shift is independent of c_t when v_t is zero.
(iv) In the case of a constant speed of sound ($c = c_s = c_t$), Eq. (28) reduces to Eq. (1).

2.3. Measurement errors by the conventional equation

In the present theory, the expected moving target speed, v_{tm}, is obtained using the conventional equation (Eq. (1)), and the difference in speed between v_{tm} and the true value v_t calculated using Eq. (28) is considered to be the measurement error.

In order to examine the estimation of such error, we introduce the parameter A as the ratio of the speed of sound around the target, c_t, to the speed of sound around the sound source, c_s [8]:

$$A \equiv \frac{c_t}{c_s}. \tag{29}$$

The true measured Doppler shift is Δf_m, where v_{tm} is obtained from Eq. (1) as

$$\Delta f_m = 2\frac{(v_s - v_{tm})}{c_s}\cdot f \tag{30}$$

Equating Δf_m and Δf_{imp} in Eq. (28), v_{tm} becomes

$$v_{tm} = \frac{v_t}{A} \tag{31}$$

Therefore, the error of the moving target speed, v_{tdif}, is obtained as

$$v_{tdif} = v_{tm} - v_t = \left(\frac{1}{A} - 1\right)\cdot v_t \tag{32}$$

From Eq. (32), the relative error of the moving speed of the target, $RE(v_{tdif})$, is

$$RE(v_{tdif}) = \frac{v_{tdif}}{v_t} = \left(\frac{1}{A} - 1\right) \tag{33}$$

Eq. (33) reveals that $RE(v_{tdif})$ decreases in inverse proportion to A, i.e., when the speed of sound around the target, c_t, is different from the speed of sound around the sound source, c_s, the relative error, $RE(v_{tdif})$, of the target speed is on the same order of magnitude as parameter A.

Since the speed of sound around the target, c_t, is generally unknown, it is not possible to compensate for the relative error, $RE(v_{tdif})$, in Eq. (33). However, it is important to recognize that this error is a systematic error that always occurs when c_t differs from c_s.

3. Experiments

In order to verify the improved Doppler shift equation, model experiments were conducted using a small water tank of size W900 mm × D450 mm × H450 mm, as shown in Fig. 6. In the experiments, the moving speed, v_s, of the sound source (transducer) was set to zero. The improved Doppler shift equation in this case is expressed as

$$\Delta f_{imp} = \frac{-2\cdot\cos\theta\cdot v_t\cdot f}{c_t}, \tag{34}$$

where θ is the angle between the direction of v_t and that of the wave propagation (i.e., the bottom line of the tank).

Fig. 7 plots the speed of sound in water against the water temperature using data from Ref. [9]. Incidentally, the speed of sound in water is strongly dependent on temperature in the range of approximately 0–60 °C, as Fig. 7 shows. The speed around the target, c_t, in Eq. (34) at an arbitrary temperature was then determined by linearly interpolating actual measurement data at intervals of 1 °C between 0 and 60 °C [9].

3.1. Experimental setup

The inner area of the tank was divided into two areas by an acrylic partition board with a thickness of 10 mm. A lead zirconate titanate (PZT) disk 20 mm in diameter molded with urethane rubber was installed in one tank as the transducer. A chain 0.9 m in length composed of aluminum spheres 2.4 mm in diameter was placed near the center of another tank as the moving target in order to avoid the influence of reflections from the walls of the tank. The distance between the transducer and the target is approximately 0.5 m. The speed of sound around the transducer, c_s, and the speed of sound around the target, c_t, were set by varying the water temperature of each tank. Hereinafter, the two partitioned areas are referred to as the transducer and target tanks.

An acoustic window 110 mm in diameter was prepared in the center of the partition board. A sheet of polyethylene plastic wrap was affixed to the window oblique to the wavefront. Chloroprene sponge rubber with a thickness of 5 mm containing small enclosed bubbles was adhered to the entire surface of the partition board, excluding the acoustic window, to provide heat insulation between the two tanks.

Before the start of the experiment, the water in both the target and transducer tanks was first warmed to 54 °C to remove air bubbles contained in the water, which was then left to cool undisturbed until returning to room temperature. During the experiments, ice was used to cool the water of the two tanks, and two 1-kW heaters were used to heat the water. The water temperatures in the two tanks were monitored using bar thermometers.

The ends of the chain used as the target were connected to the ends of a rubber fishing strap 0.2 m in length to provide tension. The chain was then fixed to two rotating gears 99 mm in diameter. The angle between the chain and the bottom of the tank was $\theta = 41.5°$, and the plane of rotation of the gears was oriented sideways, as shown in Fig. 6. The upper rotating gear was submerged in order to prevent the formation of air bubbles caused by the rotation of the gear.

In order to maintain a uniform distribution of water temperature in each tank, we operated water circulators in the tanks, which were observed using bar thermometers that measured the temperatures at three positions in the target tank, i.e., in the vicinities of the upper gear, of the target reflection point, and of the lower gear, which were approximately the same. Likewise, the water temperatures at three positions in the transducer tank, i.e., in the vicinities of the transducer upper position (near water surface), the transducer position, and the transducer lower position (near tank bottom), were measured to be the same.

An electric motor was connected directly to the rotating shaft of the upper gear, and the speed, v_t, of the target was varied by changing the rotation speed of the motor. The rotation speed of the motor was measured using a handheld tachometer (SHIMPO Dt-103c).

The speed, v_t, of the target in meters per second was obtained as

$$v_t = D\cdot\pi\cdot\left(\frac{RPM}{60}\right)\cdot\left(\frac{50}{90}\right), \tag{35}$$

where $D = 99$ mm is the target rotation diameter, RPM is the measured rotation speed (min^{-1}), 90 is the number of teeth in the gears attached to the motor rotating shaft, and 50 is the number of teeth in the gears attached to the tachometer.

A tone burst pulse with a frequency of 1.99 MHz, a pulse width (PW) of approximately 0.2 ms (400 cycles), and a pulse repetition time (PRT) of approximately 40 ms was transmitted toward the target, and the echo reflected by the target was received by the same transducer. The received waveforms were converted to a digital signal at a sampling frequency of 10 MHz via an analog-to-digital (A/D) device built into a

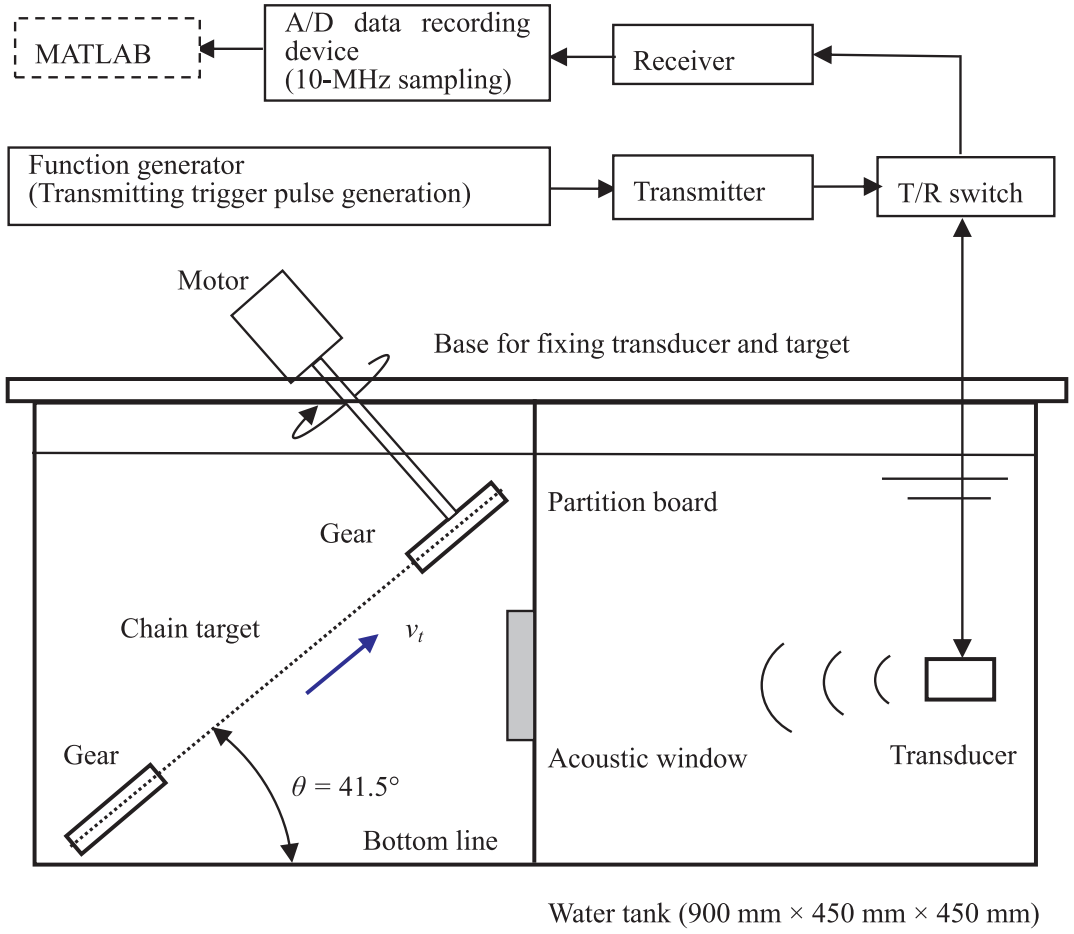

Fig. 6. Experimental setup.

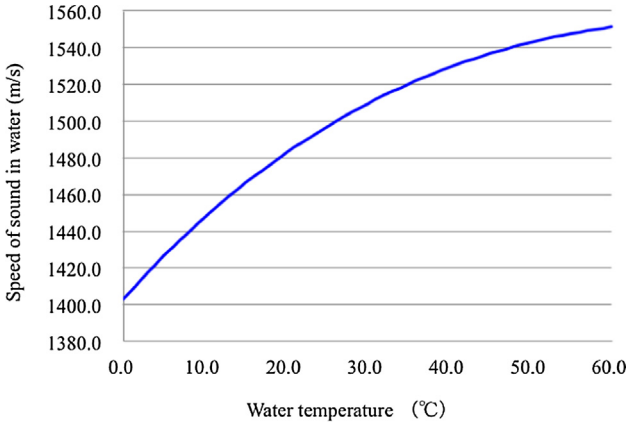

Fig. 7. Speed of sound in water versus water temperature [9].

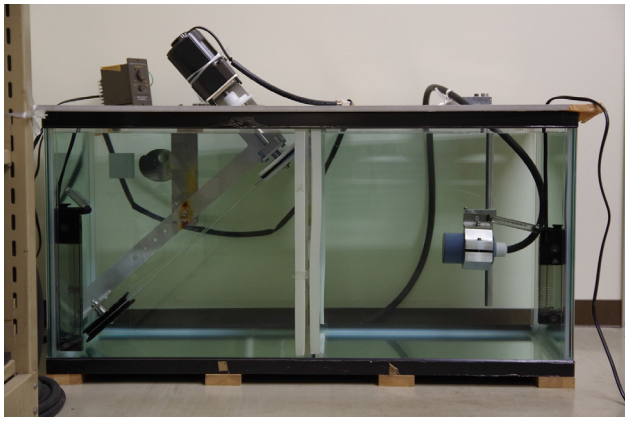

Fig. 8. Photograph of the experimental setup.

digital oscilloscope (LeCroy 6051A). The recorded data were used in the offline frequency analysis of the Doppler shift with the method described in the following section. Fig. 8 shows a photograph of the experimental setup.

Fig. 9 shows a typical received waveform. The first pulse, a, is a leakage electric signal from the transducer, and the second pulse, b, is the direct acoustic wave from the target. Pulse c and several subsequent pulses are the reflected signals from the back and side walls of the tank and the water surface. The receiver gain in the measurement system was adjusted so that the target echo signal, b, in Fig. 9 did not saturate. At that time, the leakage electric signal, a, and the reflected signal from the back wall, c, were saturated. Therefore, it is not possible to simply compare the amplitudes of b and c. The elapsed time from pulse a to pulse b was measured to be 0.67 ms. This corresponds to the actually measured distance of 0.5 m between the transducer and the target by taking into account the speed of sound of 1502 m/s at 26.9 °C. In the same way, the measured distance of 0.19 m from the target to the back wall corresponds to a time difference of 0.25 ms between pulses b and c.

3.2. Frequency analysis of received waveforms

When $\theta = 45°$, $v_t = 2.5$ m/s, and $f = 1.99$ MHz, Eq. (34) predicts that the Doppler shift generated by the change in the speed of sound as waves travel from water at 10 °C to water at 50 °C is approximately

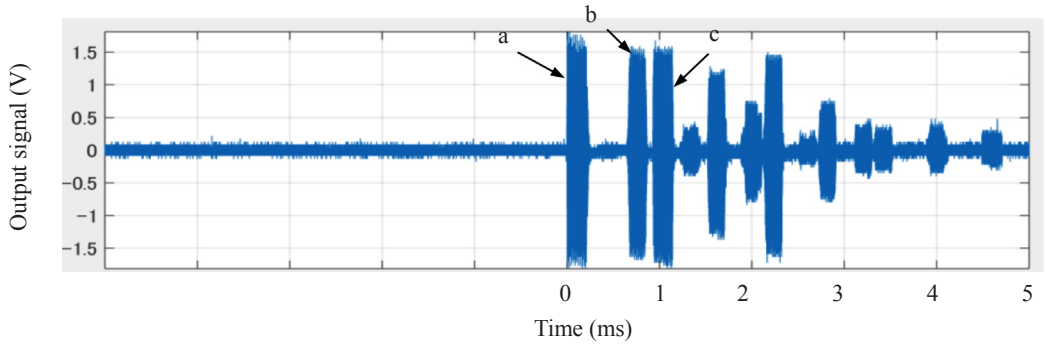

Fig. 9. Typical waveform received by the transducer. a: Leakage electric signal from the transducer, b: Echo signal from the target, c: Reflected signal from the back wall of the tank.

300 Hz. Therefore, we supposed that the accuracy of the frequency analysis (i.e., the resolution of Fourier transform) required to detect this change was approximately 10 Hz, i.e., one order of magnitude smaller than the expected change. Accordingly, a resolution of 10 Hz was obtained from the received echo waveforms using the following procedure.

(i) A section in the center of the target echo signal 0.10–0.11 ms in width (time series data with approximately 1000 sampled points) is selected from the target echo signal, which spans approximately 0.2 ms (time series data with approximately 2000 sampled points), truncating the waveforms before and after the target echo signal. The echo signal is truncated in this manner in order to avoid the influence of the transient waveforms arising from the transducer response and the characteristic reflection from the chain target.
(ii) The resolution (i.e., frequency spacing or data interval) of the fast Fourier transform (FFT) is determined by the ratio of the sampling rate in hertz to the number of samples. When the sampling rate is 10 MHz, 1 million samples are required in order to achieve a resolution of 10 Hz. Therefore, the truncated echo signal is zero-padded (i.e., zeros were added to the signal data) such that the total number of samples becomes 1 million. The zero-padding technique enhances the accuracy of estimating the frequency of a spectral peak when the data constitute a narrow band signal with a center frequency [10].
(iii) The spectrum distribution is obtained by performing a frequency analysis of the 1 million samples with the aid of MATLAB.
(iv) The peak value of the computed spectrum distribution is expected to be the center frequency, f'', of the target echo signal. Therefore, the Doppler shift is determined based on the difference between the transmission frequency, f, and the center frequency, f''.

3.3. Experimental results

3.3.1. Changing the target speed while keeping the transducer and target tanks at room temperature

While the water temperatures in the target and transducer tanks were maintained at 21.0 and 19.6 °C, respectively, the Doppler shift that occurred when the moving speed of the target, v_t, was gradually increased from 0 to 2.41 m/s was measured. The average values of 20 measured data for four target speeds of v_t = 0, 0.72, 1.58, and 2.41 m/s and the corresponding theoretical values from Eq. (34) are plotted against the moving speed v_t in Fig. 10. Fig. 10 shows that the measurement results agree with the theoretical values, with differences on the order of a few tens of hertz. The standard deviations of the four measurements were 11.4 (v_t = 0 m/s), 42.3 (0.72), 58.4 (1.58), and 74.9 (2.41) Hz, respectively.

3.3.2. Varying the water temperature in the transducer tank while keeping the target tank at room temperature

With the water temperature in the target tank maintained near room temperature (20.5–22.0 °C), the Doppler shift that occurred when the water temperature in the transducer tank was varied from 11.4 to 52.2 °C was measured. The speed of the target, v_t, was fixed at 2.41 m/s. The average values of 20 measured data for four transducer tank water temperatures of 11.4, 25.5, 39.6, and 52.2 °C and the corresponding theoretical values calculated from Eq. (34) are plotted against the water temperature in the transducer tank in Fig. 11. The vertical bars for the measurement data in the figure indicate plus and minus the standard deviations for the 20 measured data, and the standard deviation is hereinafter referred to as the variation of the measured data.

In this case, the Doppler shift, Δf, is only slightly related to the speed of sound around the transducer, c_s, and is therefore also independent of the water temperature of the transducer tank, as can be seen from Eq. (34). Fig. 11 shows that the measured Doppler shifts were independent of the temperature, demonstrating agreement with the present theory.

3.3.3. Varying the water temperature in the target tank while keeping the transducer tank at room temperature

Unlike the measurement in Section 3.3.2, the water temperature of the transducer tank was maintained at room temperature (19.0–22.0 °C). Fig. 12 shows the Doppler shift that occurred when the water temperature of the target tank was varied from 10.2 to 51.7 °C, where v_t was fixed at 2.41 m/s. The average of 20 measured data for target tank temperatures of 10.2, 24.8, 39.0, and 51.7 °C and the corresponding theoretical values are plotted against the target tank temperatures in Fig. 12.

The Doppler shift, Δf, varies with the water temperature in the target tank, reflecting its dependence on the speed of sound around the target, c_t, as indicated in Eq. (34). Fig. 12 demonstrates that the measured data varied in accordance with the theoretical values calculated from Eq. (34).

The variations of the measured data in Fig. 12 are larger than those in Fig. 11. The reason for the appearance of such large variations has not yet been determined. One of the probable causes may be non-uniformity of water temperature distributions in a local area, i.e., the fluctuations in the temperature distribution in the vicinity of the chain target, which affects the received waveform in terms of amplitude and phase, although the uniformity was actually observed by a thermometer, as mentioned in Section 3.1. Another possibility may be the existence of invisible floating small bubbles in water that generate unnecessary echo waves. The clarification of these reasons is underway.

4. Conclusions

The present study has improved the conventional Doppler shift equation by considering the variation in the speed of sound along the propagation path based on the expansion and contraction of the pulse

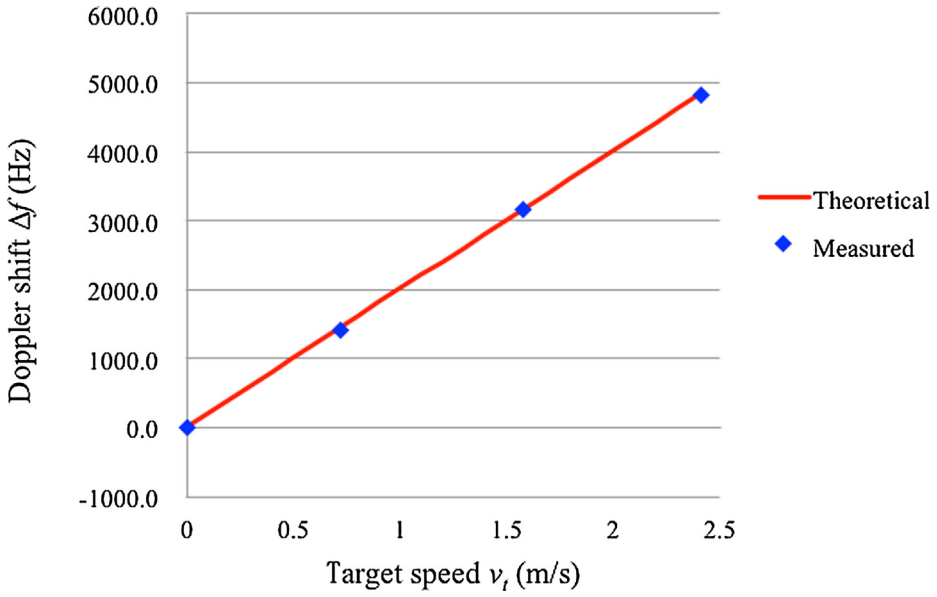

Fig. 10. Theoretical and measured Doppler shift Δf plotted against the target speed v_t.

time width that occurs during propagation. The proposed improved Doppler shift equation reveals that both the speed of sound at the sound source position and that at the target position affect the Doppler shift. The measurement errors caused by the use of the conventional Doppler shift equation were also derived in comparison with the improved Doppler shift equation. When the speed of sound near the target differs from that near the sound source, the relative error of the target moving speed is expected to be on the same order of magnitude as the ratio of the speed of sound near the target to that near the sound source. Furthermore, model experiments to validate the derived improved Doppler shift equation were conducted. The measured data for the speed of sound and the Doppler shift showed agreement with the derived improved Doppler shift equation.

The improved Doppler shift equation indicates that the measured Doppler shift includes information about the speed of sound near the target. The results of the present study are expected to make feasible the remote measurement of the speed of sound near a target.

Acknowledgements

The authors would like to express their appreciation to Mr. Masami Hasegawa and Mr. Hideki Horiuchi of Japan Radio Co., Ltd., for their cooperation in preparing the experiments, to Mr. Kohjiro Imasato of Japan Radio Co., Ltd., for his advice on frequency analysis using MATLAB, and to Mr. Kenji Sekimori of Ueda Japan Radio Co., Ltd., for his assistance in preparing the ultrasonic transducer for the experiments.

Declarations of interest

None.

Funding

This research did not receive any specific grant from funding

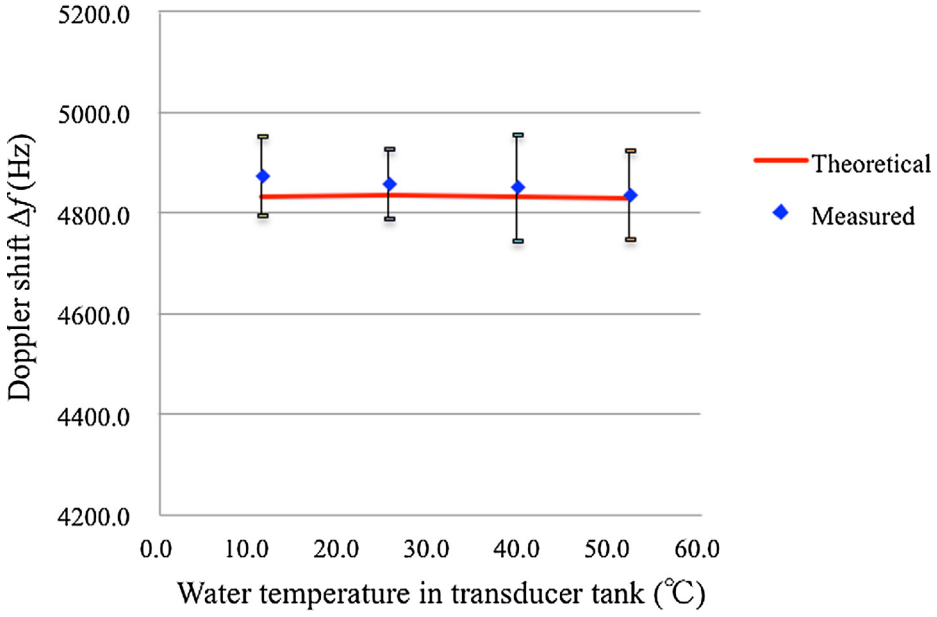

Fig. 11. Theoretical and measured Doppler shifts Δf plotted against the water temperature in the transducer tank.

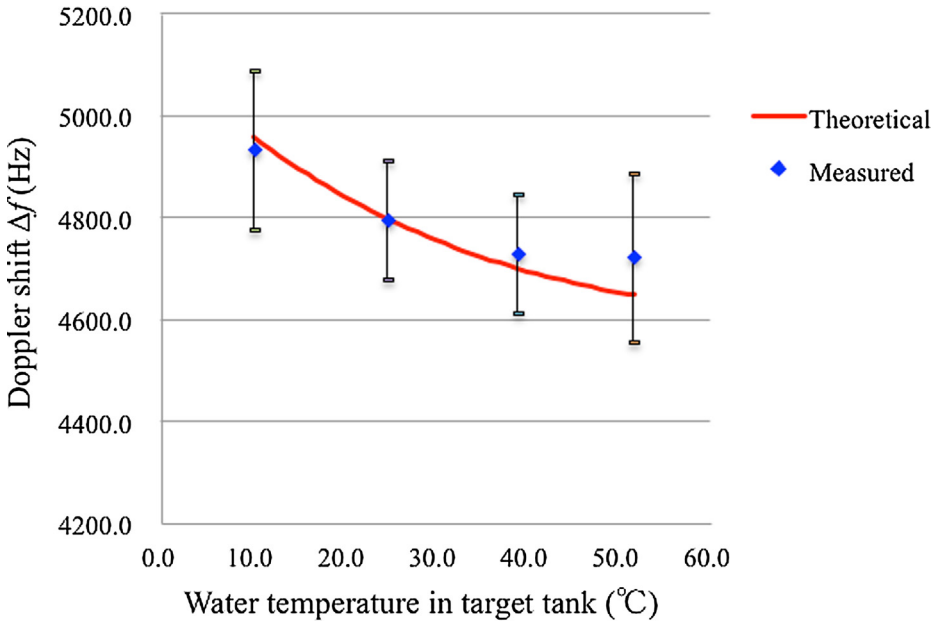

Fig. 12. Theoretical and measured Doppler shifts Δf plotted against the water temperature in the target tank.

agencies in the public, commercial, or not-for-profit sectors.

References

[1] F.D. Rowe, J.W. Young, An ocean current profiler using Doppler sonar, IEEE Proc. Oceans 79 (1979) 292–297.
[2] J.W. Young, F.D. Rowe, B.H. Brumly, S.E. Bradley, Trends in velocity log technology at RD instruments, in: IEEE Proc. 1998 Workshop on Autonomous Underwater Vehicles, 1998, pp. 89–101.
[3] R.D. Teledyne, Instruments, acoustic Doppler current profiler. Principles of operation: A practical primer 33 (2011).
[4] K.V. Mackenzie, Nine-term equation for sound speed in the oceans, J. Acoust. Soc. Am. 70 (1981) 807–812.
[5] A. Radosevic, R. Ahmed, T.M. Duman, J.G. Proakis, M. Stojanovic, Adaptive OFDM modulation for underwater acoustic communications: design considerations and experimental results, IEEE J. Ocean. Eng. 39 (2) (2014) 357–370.
[6] C.S. Clay, H. Medwin, Acoustical Oceanography: Principles and Applications, John Wiley & Sons, 1977, pp. 334–338.
[7] S. Tanaka, T. Kamakura, H. Nomura, Effect of sound speed and sea current during propagation on Doppler shift, IEEE IUS 2016, Paper ID 1197 (2016).
[8] S. Tanaka, H. Nomura, T. Kamakura, Measurement errors in ultrasonic Doppler devices caused by variation in the speed of sound along the propagation path, UACE 2017 (2017) 259–264.
[9] M. Greenspan, C.E. Tschiegg, Tables of the speed of sound in water, J. Acoust. Soc. Am. 31 (1959) 75–76.
[10] S.L. Marple Jr., Digital Spectral Analysis with Applications, Prentice-Hall Inc, 1987, pp. 43–45.